Electrical Characterisation of Defects in Cu-rich Grown $CuInSe_2$ Solar Cells

Tobias Bertram, Valérie Deprédurand, and Susanne Siebentritt

***Abstract*—We study defects in $CuInSe_2$ (CIS) grown under Cu-excess. Samples with different Cu/In and Se/metals flux ratios were characterized by thermal admittance spectroscopy (TAS), capacitance-voltage measurements (CV) and temperature dependent current voltage measurements (IVT). All samples showed two different capacitance responses, which we attribute to defects with energies around 100 and 220 meV. Plus the beginning of an additional step that we attribute to a freeze-out effect. By application of the Meyer-Neldel rule, the parameters of the two defects can be assigned to two different groups, both lying within the energy region of the so-called 'N1-defect' that has been observed for Cu-poor absorbers.**

***Index Terms*—Admittance measurement, Capacitance measurement, Thin Film PV Device Properties and Modeling, Photovoltaic cells**

I. Introduction

Commercial and record lab cells based on Cu(In, Ga)Se_2 are manufactured under Cu-poor conditions; therefore most in-depth studies are confined to this type of material. However, by growing CIGS (or its ternary CIS) under an excess of copper it becomes possible to form a stoichiometric chalcopyrite phase with the surplus of Cu being incorporated in a secondary Cu_xSe phase, which preferably aggregates at the surface. The overall Cu/In ratio of this whole film is then above unity. Due to its high conductivity, the secondary phase has to be removed from the surface by KCN etching before finishing the absorber into a solar cell. In the following, solar cells and absorbers made from CIS without Ga are examined. These were grown under Cu-excess conditions and etched. So they are referred to as 'Cu-rich'. This material provides a multitude of benefits over the standard Cu-poor grown material [1]: Spectral photoluminescence measurements at fixed excitation densities can quantify the quasi-Fermi-level splitting. Previous studies [2] utilizing this method have shown that Cu-rich absorbers show a higher amount of splitting compared to the Cu-poor material and therefore have the potential to achieve higher open-circuit voltages. Furthermore Hall measurements on $CuGaSe_2$ (CGS) reveal increased carrier mobilities for Cu/In ratios above stoichiometry [3], which if it translates to CIS can improve carrier collection, resulting in better short-circuit currents (J_{SC}) than for the Cu deficient material. But although Cu-poor devices reach efficiencies up to 15 % [4], in general Cu-rich devices show much lower efficiencies, because they suffer from interface recombination [5]. Nonetheless, it is possible to mitigate this limitation by applying a surface treatment in order to form a Cu-poor layer at the absorber surface [6] [7] [8]. This surface treatment allowed us to produce Cu-rich devices as efficient as our Cu-poor ones [9]. Here, we study the defects occurring in Cu-rich CIS, grown with different Cu/In and Se/Me flux ratios. It was shown previously [10] that a lower Se flux has a positive impact on solar cell efficiency, as well as influences on X-ray diffraction and photoluminescence spectra. It has been shown that the selenium supply during growth has a high impact on the intrinsic doping of the Cu-rich absorbers and can even lead to a type inversion for very low Se environments [10] [11]. Here we investigate the electronic structure of deep defects within the absorber. Thermal admittance spectroscopy was employed in order to achieve this goal. This method allows the characterization of deep states within the absorber [12] by changing the applied AC bias frequency and sample temperature. The measurement results were subsequently evaluated by modelling the defect distribution according to Walter *et al.* [13], which gives insights into the defects' activation energies, capture coefficients and concentrations within the sample. In the case that the Fermilevel is not pinned at the absorber surface it is possible to distinguish bulk from interfacial states by applying a small DC reverse bias [14]. Capacitance-Voltage measurements were used to measure the devices' doping and built-in voltages; these are crucial parameters for the evaluation according to Walter *et al.* [13]. To gauge the influence of the series resistance on the admittance spectrum, temperature dependent current-voltage measurements complemented the capacitive methods shown here.

The authors are with the Laboratory for Photovoltaics, Physics and Material Science Research Unit, University of Luxembourg, L-4422 Belvaux, Luxembourg e-mail: (tobias.bertram@uni.lu; validep@hotmail.com; susanne.siebentritt@uni.lu).

II. Sample Preparation

The absorbers of the cells were grown at 590 °C by a 1-stage physical vapour deposition (PVD) co-evaporation process on a Mo-coated soda-lime glass substrate in an MBE System. Two different series at fixed Cu and In fluxes, as measured by quartz crystal microbalance (QCM), were prepared to study the influence of the Se pressure. The two series were controlled to exhibit a low and a high Cu-excess, respectively. The flux of Se was measured by a beam flux monitor (BFM) and controlled by the valve of the Se source. Within each series with fixed Cu/In flux ratio the Se/Me flux ratio was varied between 12 and 6. More details regarding the growth can be found in reference [10]. To evaluate the Cu/In ratios of the absorbers, energy dissipative X-ray spectroscopy (EDX) measurements were performed before the etching step. It was observed that

the Cu/In ratio was dependent on the Se flux during growth, leading to higher Cu/In ratios for Se-poorer environments regardless of the fixed Cu and In fluxes. Therefore the Cu/In ratios in the films were between 1.2 and 1.5 for the low Cu/In series and between 1.8 - 2.0 for the high one. All samples were selectively etched by KCN to remove the secondary Cu_2Se phase, before deposition of the n-CdS buffer layer by chemical-bath deposition. Afterwards they were sent to the Helmholtz Zentrum Berlin for finishing with the i- and n-ZnO-window layer and Al:Ni grid front contacts.

III. Capacitance-Voltage measurements

CV measurements were performed by measuring the capacitance of the cell under an applied DC-bias utilizing a LCR-meter with AC frequencies up to 1 MHz at room temperature. The main goal is to measure the doping density N_A of the absorber and the built-in voltage V_{bi}. From N_A & V_{bi} we can calculate the space-charge region width d_{SCR} and its contribution C_{SCR} to the measured capacitance. To prevent an overload of the setup due to high currents, the samples had to be cut into small pieces with areas of approximately $0.2\,\mathrm{cm}^2$. Evaluation was then carried out through linear extrapolation of the Mott-Schottky plot [12], which is defined as the square of the inverse capacitance over the applied bias yielding N_A and V_{bi}. The first parameter is anti-proportionally linked with the slope, while the second one is constituted by the intercept with the bias-axis. This can easily be derived from the formula for the one-sided pn-junction [12]

$$C = \sqrt{\frac{\varepsilon\varepsilon_0 e N_A}{2\left(V_{bi} - V_{app}\right)}}. \tag{1}$$

Furthermore d_{SCR} can be estimated from the capacitance of the linear fit at zero-bias, by applying the parallel plate capacitor model for the SCR (with $\varepsilon = 12$ [15]). Only data points at small forward biases were factored in for the linear fit. This methodology was chosen to diminish the capacitance contribution of deep defects on the measurements [12]. Under reverse bias those defects cross the Fermi-level which increases the measured capacitance, thereby lowering the slope. The extracted carrier density is then not equal to the doping, but rather the combined doping and defect densities, which also increases the built-in voltage to unphysical high values. Also as described by Scofield *et al.* [20], when evaluating CV data it is advised to pay attention to the measured phase angle ϑ_m between the measured capacitance and conductance, as the capacitance results are deemed unreliable for values smaller than 20°.

IV. Admittance measurements

For the admittance measurements the samples were mounted in a closed cycle liquid helium cryostat. The temperature is measured by a silicon diode, glued to a glass substrate close to the sample. Capacitance and conductance values were monitored with the same LCR-meter as for CV. The measurements were performed on the full sized samples, with areas of about $0.5\,\mathrm{cm}^2$. Measurement and evaluation of the activation energies (E_A) and emission coefficient (ξ_0) were carried-out in terms of the standard analysis for deep defects [12]. Capacitance steps are usually analysed in terms of the emission rate of deep defects, see eq. (2). Because of the temperature dependence of the emission rate, it becomes possible to probe different defect energies within the space charge region (SCR), by decreasing the temperature of the cell. Levels which cross the Fermi-level within the SCR can be charged and uncharged by an AC bias signal. At increased frequencies, higher than the emission rate of the trap, this contribution is eliminated - resulting in a capacitance step with an inflection point at a characteristic frequency (f_0), which is described by [15]:

$$f_0 = \frac{\nu_0}{\pi} e^{\frac{-E_A}{kT}} \tag{2}$$

$$\nu_0 = \xi_0 T^2 \tag{3}$$

To quantify E_A and ξ_0 of these defects one either plots the natural logarithm of f_0 over the inverse temperature in an Arrhenius graph, or [13] models the density of states (DOS) of the defect to fit the $\frac{dC}{d\omega}$ spectrum by the formula, hereafter referred to as Walter analysis:

$$N_t\left(E_A\right) = -\frac{V_{bi}^2}{d_{SCR}\left[qV_{bi} - \left(E_{fp\infty} - E_A\right)\right]} \cdot \frac{dC}{d\omega} \cdot \frac{\omega}{kT} \tag{4}$$

The first method is a quick and simple way to gain insight into the desired defect parameters that manifest themselves in the slope and intercept of the linear regression of the data points, while the second one requires some estimates for input parameters like the bulk Fermi-energy ($E_{fp\infty}$), the SCR width (d_{SCR}) and built-in voltages (V_{bi}), but also offers the added benefit of giving an estimate of the concentration of the trap states (N_T) and the broadness in energy (W_{FWHM}) of their distribution. The required parameters are obtained by CV measurements as described in the previous section. Once all the values are inserted into the formula, the activation energy can be extracted by adjusting the characteristic frequency ν_0 until the defect densities at each given temperature line up. Both evaluation methods assume the capacitance response to originate from bulk defects within the p-type absorber. Obviously the complex structure of a solar cell leads to other phenomena, which can show a similar contribution, namely localized defects at the absorber-buffer interface [16], the response of the equivalent circuit with a thermally activated series resistance R_S [17], a back-contact barrier [18] or mobility freeze-out [19]. The TAS measurement gives further insight into the character of the signals. TAS steps which are due to deep defects occur above the SCR capacitance while series resistance, barrier or freeze-out related steps occur usually below the C_{SCR}. TAS measurements under a small reverse bias may in some cases help to tell an interfacial from a bulk defect. The latter will have the same E_A regardless of bias, but - if the Fermi-level is not pinned - an interface state will occur at a different energy [14]. For the thermally activated series resistance R_S, as described in [17] the shunt R_{SH} and series resistance form a circuit, which responds to

the measurement signal. This response C_{res} can be modelled from the low frequency capacitance C_{lf} above the step in question:

$$C_{res} = \frac{C_{lf}}{\left(1 + \frac{R_S}{R_{SH}}\right)^2 + (\omega R_S C_{lf})^2} \quad (5)$$

At low temperatures the series resistance increases, up to the point where $\omega R_S C_{lf}$ becomes significantly large for high frequencies, resulting in a reduction of the capacitance similar to a defect response. If the shunt and series resistances are known from complementary IVT measurements, one is able to model this equivalent circuit, by setting C_{lf} as the measured capacitance at low frequencies and calculate at which frequency this response sets-in for each temperature. Above this frequency the capacitance data is dominated by the series resistance, so it can not be evaluated as described by equation 4. However, it can still contain information about defects, if the thermally activated behaviour of R_S is due to carrier freeze-out, or about barriers, if the activated R_S behaviour is due to a transport barrier. A mobility freeze-out leads to a non-linear behaviour of the Arrhenius plot, which can be straightened out by plotting $\ln\left(\omega T^{\frac{1}{2}}\right)$ over $T^{-\frac{1}{4}}$ [19] if the low temperature mobility is dominated by variable range hopping. Also it should be the last step in the admittance spectrum and go down to the geometric capacitance C_{geo} (lowest dashed blue line in fig. 2) of the fully depleted absorber.

V. Measurement Results

The room temperature CV measurements were evaluated as described in sec. III via Mott-Schottky plots. As reported previously [10] a correlation between Se supply during growth and doping density was found, the value of which was $3 \cdot 10^{16}\,\mathrm{cm}^{-3}$ for the high Se flux samples and could be reduced to $1 \cdot 10^{16}\,\mathrm{cm}^{-3}$ for the low Se flux samples. In fig. 1 the measurement results are shown for the high Cu/In series. All the results for the extracted parameters from the CV measurements are shown in table I. Due to the still rather high doping of the absorbers the SCRs are rather short. The built-in voltages in the range of 0.55 - 0.75 V showed reasonable values below the band gap energy. However, we can not fully exclude the possibility that there still is a defect contribution from a deep defect within the sample, therefore the values for N_A, V_{bi} and C_{SCR} might be slightly lower than the measured values.

TAS measurements on the Cu-rich samples show three separate capacitance steps, as is depicted for a typical measurement in fig. 2. They are labelled step 1 to 3 in order of their appearance with decreasing temperature, step 1 always shows the smallest capacitance drop, while step 2 and 3 are about the same height, assuming that step 3 ultimately drops to C_{geo}. Step 1 and 2 are fully visible, but step 3 cannot be fully resolved due to the limitation of the measurement frequency and temperature.

The signal above C_{SCR} for the higher measurement temperatures is due to a deep defect which leads to the flattening of

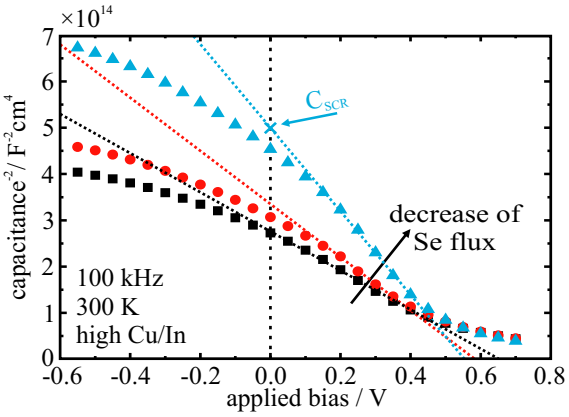

Fig. 1. Mott-Schottky plot for the high Cu/In series for evaluation of the doping density.

TABLE I
Absorber parameters as extracted from capacitance-voltage measurements

Cu/In	Se	N_A cm^{-3}	U_{bi} V	d_{SCR} nm	C_{SCR} $nFcm^{-2}$
high	low	$1.3 \cdot 10^{16}$	0.55	232	45
	mid	$2.1 \cdot 10^{16}$	0.58	190	55
	high	$2.9 \cdot 10^{16}$	0.65	172	60
low	low	$1.1 \cdot 10^{16}$	0.58	262	40
	mid	$1.3 \cdot 10^{16}$	0.59	240	43
	high	$2.3 \cdot 10^{16}$	0.75	206	50

the CV curves for reverse bias. Since it is only partly observed, no inflection points are detected, we do not discuss this signal further. We have performed IVT measurements and extracted the resistances through a fit of the current-voltage curves at each given temperature with a one-diode model. From this, we fit the circuit response of the series resistance as described in section IV. The third step in fig. 2, appears in the region where the circuit response dominates the capacitance spectrum [17]. We correlate this to the rise in R_S which can be due to a barrier, carrier or mobility freeze-out, but it is only observed partly, therefore it cannot be analysed further.

The two remaining, fully resolved steps (1 and 2) are analysed further in the following. The behaviour depicted in fig. 2 is typical for all measured samples independent of their Cu/In or Se/Me ratio. The capacitance contribution of deep traps adds to the capacitance of the depletion region, in contrast to shallow defects, freeze-outs and barriers, which subtract from it. As described previously we can get C_{SCR} from CV measurements, in fig. 2 this has been plotted as the upper blue line.

From fig. 2 it becomes directly apparent, that the three steps appear below the C_{SCR} and therefore seem to not originate from deep defects. This is true for all samples, as becomes obvious by comparing C_{SCR} given in tab. I and the capacitance above step 1 and 2 (denoted C_{up} in tab. II, black dashed lines in fig. 2). This way of analysing capacitance spectra is not usually done in the CIS literature, therefore we would like to stress that admittance results should be

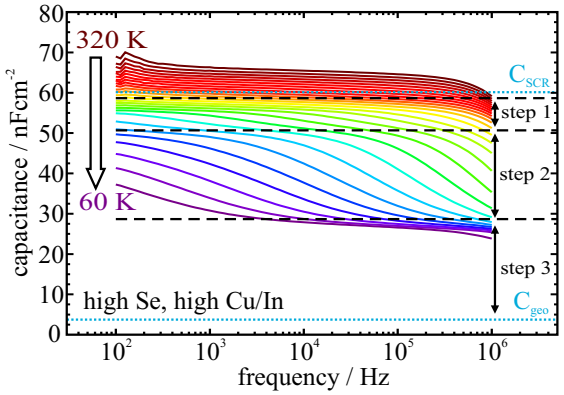

Fig. 2. Typical admittance spectrum with three capacitance steps exemplary for the studied samples. The sample that yielded the depicted data was grown with a high Cu/In ratio under high Se.

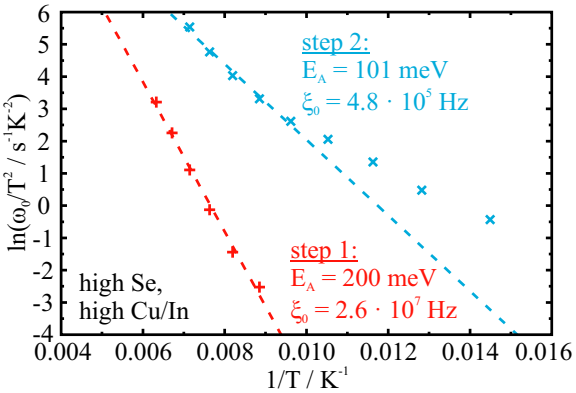

Fig. 3. Typical Arrhenius plot, as exemplary for the sample with a high Cu/In ratio and high Se during growth.

supplemented by CV data. In the original paper by Walter *et al.* [13], the evaluation on the CIS sample has been performed on a capacitance step below C_{SCR}. Although in this case the prerequisites of the Walter analysis are not strictly fulfilled, the classical analysis can be used to compare the contribution and width of various capacitance signals among the samples and with literature.

The evaluation via Arrhenius plot (see figure 3) was performed on measurements without bias and under a small reverse voltage of -0.2 V. The capacitance step 1 forms a straight line, while the data points for step 2 show a deviation from the linear behaviour towards lower temperatures for all samples.

The extracted activation energies are in the range of 200 to 250 meV for step 1 and for the linear, high temperature part of step 2 between 50 - 130 meV depending on the sample. All values are unchanged under bias. The measured energies for step 1 are too high for a doping defect , since the Fermi-level would need to be above that value. Also a back-contact barrier with such a high activation energy is unlikely. It is possible, that the measured signal corresponds to an interface defect, but we would have to assume Fermi-level pinning at the interface, because of the signal not shifting with bias. Identifying step 1 as a deep defect is the conclusion for which one has to make the least assumptions. It is rather likely, that it has a contribution to the CV measurements, that can not be fully resolved by applying a forward bias, this would lead to a measured C_{SCR} that is too high. We presume that C_{up} for this defect is actually above the true C_{SCR}, therefore step 1 could very well be a deep defect in Cu-rich CIS.

To explain the bending of the Arrhenius plot for step 2, different temperature dependencies were tested, but neither yielded a straight line. Therefore it is probably neither the response of a barrier or a mobility freeze-out due to variable-range hopping [19], because this should be characterized by a linear $T^{-\frac{1}{4}}$-plot. Since the measured energies are much lower than for step 1 it is probably also lower than the Fermi-energy, allowing for this step to be due to the freeze-out of a doping defect. PL studies of Cu-rich CIS absorbers find three different energies for the doping defects in CIS. A $\sim$ 10 meV donor and

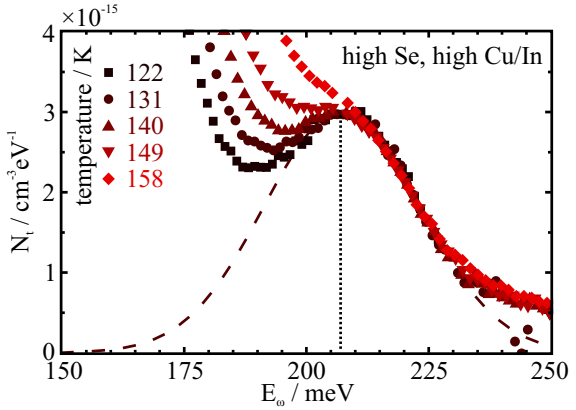

Fig. 4. Modelling of the defect DOS for step 1 in the sample with a high Cu/In ratio and high Se during growth.

additional to that three acceptor levels: for near stoichiometry one with an E_A of 40 meV (labelled 'A1'), for Cu-rich of 60 meV ('A2') [21] and a third one at 100 meV independent of Cu-excess ('A3' in [22]). These are well within the measured energy range, the best explanation of step 2 therefore might be the freeze-out of either 'A2', 'A3', or both together.

As stated previously, for comparability we will also show the Walter evaluation. Typical results for the first and the second capacitance step are shown in figures 4 & 5, respectively.

Furthermore all the extracted parameters from the fitting are given in table II. The activation energy and frequency values are usually close to the ones extracted from the Arrhenius plot, especially for step 1. This rather well fitting of its density of states with the Walter analysis and the straight Arrhenius plot might support the conclusion, that step 1 actually is a deep trap and not an interface defect. But in some cases for the second step there is a high discrepancy between the two evaluation methods. This can be attributed to the non-linearity of the characteristic frequencies in regard of the energy axis, which results in an ambiguity in the activation energy range and causes this difference. The DOS was then fitted assuming a Gaussian shaped defect distribution, which yielded the width (W_{FWHM}) and concentration (N_T) of both steps. The concentration was derived from integration of the area under

TABLE II
DEFECT PARAMETERS FOR THE TWO CAPACITANCE RESPONSES IN ADMITTANCE MEASUREMENTS

		Arrhenius plot		Walter Analysis				
Cu/In	Se	E_A meV	ξ_0 $s^{-1}K^{-2}$	E_A meV	ξ_0 $s^{-1}K^{-2}$	N_T cm^{-3}	W_{FWHM} nm	C_{up} $nFcm^{-2}$
high	low	253	$1.6 \cdot 10^9$	245	$2.0 \cdot 10^9$	$1.6 \cdot 10^{14}$	49	43
		128	$1.2 \cdot 10^6$	116	$8.0 \cdot 10^5$	$2.6 \cdot 10^{14}$	49	32
	mid	252	$7.0 \cdot 10^8$	247	$1.0 \cdot 10^9$	$1.2 \cdot 10^{14}$	37	55
		81	$9.9 \cdot 10^4$	78	$1.0 \cdot 10^5$	$5.5 \cdot 10^{14}$	31	46
	high	200	$2.6 \cdot 10^7$	207	$1.0 \cdot 10^8$	$1.2 \cdot 10^{14}$	44	59
		101	$4.8 \cdot 10^6$	58	$1.0 \cdot 10^4$	$6.7 \cdot 10^{14}$	41	51
low	low	201	$3.7 \cdot 10^7$	192	$4.0 \cdot 10^7$	$1.4 \cdot 10^{14}$	46	39
		101	$5.4 \cdot 10^5$	79	$1.2 \cdot 10^5$	$4.5 \cdot 10^{14}$	53	30
	mid	209	$5.4 \cdot 10^7$	212	$1.4 \cdot 10^4$	$9.2 \cdot 10^{13}$	41	41
		75	$8.8 \cdot 10^4$	62	$4.0 \cdot 10^5$	$3.8 \cdot 10^{14}$	38	34
	high	216	$1.5 \cdot 10^8$	192	$4.0 \cdot 10^7$	$9.1 \cdot 10^{13}$	49	44
		54	$1.4 \cdot 10^4$	46	$1.0 \cdot 10^4$	$5.6 \cdot 10^{14}$	34	39

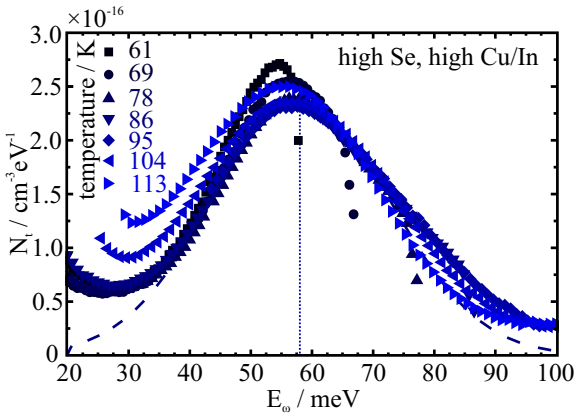

Fig. 5. Modelling of the defect DOS for step 2 in the sample with a high Cu/In ratio and high Se during growth.

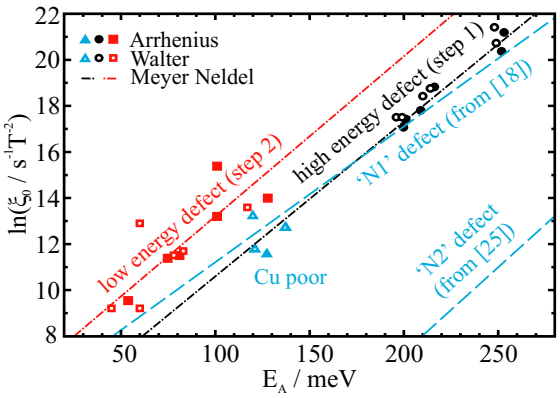

Fig. 6. Comparison between newly measured defect energies and results, published in the literature.

the Gaussian curve. Therefore the values can be overestimated for steps that are close to each other and intersect. Charting of the defect energies over the Se abundance during growth of the absorbers shows no correlation, in contrast to the strong influence of the Se pressure on the doping [10]. We attribute step 2 to a doping defect. Its much lower density N_T calculated from the Walter method ($3 \text{-} 7 \cdot 10^{14}\,\text{cm}^{-3}$) compared to N_A from CV measurements ($1 \text{-} 3 \cdot 10^{16}\,\text{cm}^{-3}$) seems to contradict this assignment. However, since there are up to three different acceptor levels in Cu-rich CIS, step 2 could be related to only one of them, while the others are too shallow to be measured with TAS but contribute to N_A.

Even though all the samples showed similar responses, the values of E_A and ξ_0 varied in between samples, seemingly uncorrelated to the Se environment during absorber growth. This strong variation of parameters is generally reported for electrical measurements and shows a linear dependency when plotted as the logarithm of ξ_0 over the associated activation energy using thermal activation for each capacitance step. This Meyer-Neldel plot, is often used to compare phenomena, which are related in their activation behaviour. The variation of ξ_0 as a function of E_A is usually explained in terms of multi-excitation entropy [23]. Admittance steps can be grouped together and should show a linear correlation if they originate from the same activated process. The slope of the linear fit is then related to the underlying activation pathway: for example a defect that captures holes from the valence band through phonon scattering should yield a slope of the phonon energy times the phonon-hole coupling constant [23]. Figure 6 shows the Meyer-Neldel plot for the measured capacitance steps.

It becomes directly apparent, that the two measurement signals form rather distinct groups that do not intermix. We can say that the nature of the activation process of both signals are very similar, because the Meyer-Neldel lines through both groups exhibit very similar slopes. We also compared the Meyer-Neldel lines to those already published in literature. In their 2013 paper, Krysztopa *et al.* gathered a comprehensive overview for various chalcopyrites including Cu-rich $CuInSe_2$, all measured with a multitude of different methods [24]. They investigated polycrystalline CIS solar cells, covering a range from Cu-poor to rich and also surveyed the literature for similar measurements. This resulted in an aggregated plot of

different groups of defects commonly referred to as 'N1' and 'N2' (the latter is referred to as 'E4' in the cited work), which are widely observed and published. Figure 6 shows our results for the Cu rich material in addition to the Meyer-Neldel lines for 'N1' [18] and 'N2' [24]. Primarily it becomes apparent, that neither of the newly detected signals corresponds to 'N2', which appears in a region of higher E_A and lower ξ_0 values. But on the other hand, both of these signals could reasonably be assigned to 'N1' with step 1 at higher energies being closer to the line. In contrast to our new findings however, the literature results were measured on Cu-poor samples. To compare to this literature, we also made a series of Cu-poor samples, with similar fluxes of Se and Cu/In ratios in between 0.92 and 0.98, i.e. slightly below stoichiometry. Admittance measurements on them show no high energy signal, but the second, with a low E_A is shifted to lower ξ_0's, thereby falling on the literature 'N1' line. The discrepancy between this signal in Cu-rich and Cu-poor absorbers can be explained by the higher doping in the Cu-rich material. This results in a higher electric field and due to this the thermal emission rate increases, shifting the line upwards within the Meyer-Neldel graph [25]. Therefore we propose, that the second step (with lower E_A, visible in all the samples Cu-poor and Cu-rich) is the same defect that also shows up in PL measurements at 100 meV ('A3', [22]), and this could be one explanation for the 'N1' signal.

VI. Conclusion

This study's aim was to shine light on the defects within Cu-rich CIS solar cells. To achieve this, samples with different Cu/In and Se/Me ratios were grown and analysed. The Se environment during growth had a profound influence on the doping density, while it had little effect on the defects' parameters visible by admittance spectroscopy. The comparison with the literature reveals two signatures, both similar to the so-called 'N1' defect. We find that step 1 is best explained as a signal due to a deep defect, while step 2 is attributed to the freeze out of a doping defect. It could be the defect 'A3', which is reported for both Cu-rich and poor samples.

Acknowledgment

As part of the CURI project this research was funded by the Fonds national de la Recherche Luxembourg, which is gratefully acknowledged. The authors want to thank M. Thévenin (University of Luxembourg), M. Kirsch (Helmholtz Zentrum Berlin) for EDX measurements and finishing of the solar cells and T. Schuler for technical support. And Prof. Margaret Igalson from the Warsaw University of Technology for discussions about electrical measurements. We are also grateful for the possibility to use of the EDX setup of Luxembourg Institute of Science and Technology.

References

[1] S. Siebentritt, L. Gütay, D. Regesch, Y. Aida and V. Deprédurand, "Why do we make Cu(In,Ga)Se_2 solar cells non-stoichiometric?", *Sol. Energ. Mat. Sol. Cells* vol. 119, pp. 18–25, 2013.

[2] L. Gütay, David Regesch, J. K. Larsen, Y. Aida, V. Deprédurand and S. Siebentritt., "Influence of copper excess on the absorber quality of $CuInSe_2$", *Appl. Phys. Lett.*, vol. 99, pp. 151912-1–151912-3, 2011.

[3] A. Gerhard, W. Harneit, S. Brehme, A. Bauknecht, U. Fiedeler, M.Ch. Lux-Steiner and S. Siebentritt, "Acceptor activation energies in epitaxial $CuGaSe_2$ grown by MOVPE", *Thin Solid Films*, vol. 387, pp. 67–70, 2001.

[4] J. A. M. AbuShama, R. Noufi, S. Johnston, S. Ward, and X. Wu, "Improved performance in $CuInSe_2$ and surface-modified $CuGaSe_2$ solar cells", *Proceedings 31st IEEE PVSC Conference*, pp. 299-302, 2005.

[5] M. Turcu, O. Pakma and U. Rau, "Interdependence of absorber composition and recombination mechanism in Cu(In,Ga)$(Se,S)_2$ heterojunction solar cells", *Appl. Phys. Lett.*, vol. 80, pp. 2598–2600, 2002.

[6] V. Deprédurand, Y. Aida, J. Larsen, T. Eisenbarth, A. Majerus and S. Siebentritt, "Surface treatment of solar cells grown under Cu-excess", *Proceedings of the 37th IEEE Photovoltaic Specialists Conference*, pp. 874–877, 2011.

[7] Y. Aida, V. Deprédurand, J.K. Larsen, H. Arai, T. Eisenbarth, M. Kurihara, A. Majerus, N. Fèvre and S. Siebentritt, "Surface treatment of solar cells grown under Cu-excess", *Proceedings of the 26th European Photovoltaic Solar Energy Conference and Exhibition*, pp. 2855–2859, 2011.

[8] Y. Aida, V. Deprédurand, J.K. Larsen, H. Arai, , D. Tanaka, M. Kurihara and S.Siebentritt, "Cu-rich $CuInSe_2$ solar cells with a Cu-poor surface", *Prog. Photovolt: Res. Appl.*, vol. 23, pp. 754–764, 2014.

[9] T. Bertram, V. Deprédurand and S. Siebentritt, "In-Se surface treatment of Cu-rich grown $CuInSe_2$", *Proceedings of the 40th IEEE PVSC Conference*, pp. 3633–3636, 2014.

[10] V. Deprédurand, T. Bertram, D. Regesch, B. Henx and S. Siebentritt, "The influence of Se pressure on the electronic properties of $CuInSe_2$ grown under Cu-excess", *Appl. Phys. Lett.*, vol. 105, pp. 172104-1–172104-5, 2014.

[11] P. Migliorato, J. L. Shay, H. M. Kasper, S. Wagner, "Analysis of the electrical and luminescent properties of $CuInSe_2$", *J. Appl. Phys.*, vol. 46, pp. 1777–1782, 1975.

[12] P. Blood and J.W. Orton, *The Electrical Characterization of Semiconductors: Majority Carriers and Electron States*, Chapters: 5, 6 & 9. New York, NY, USA: Academic, 1992.

[13] T. Walter, R. Herberholz, C. Müller and H.-W. Schock, "Determination of defect distributions from admittance measurements and application to Cu(In,Ga)Se_2 based heterojunctions", *J. Appl. Phys.*, vol. 80, pp. 4411–4420, 1996.

[14] R. Herberholz, M. Igalson and H.-W. Schock, "Distinction between bulk and interface states in $CuInSe_2$/CdS/ZnO by space charge spectroscopy", *J. Appl. Phys.*, vol. 83, pp. 318–325, 1998.

[15] R. Scheer, H.-W. Schock, *Chalcogenide Photovoltaics*. New York, NY, USA: Wiley, 2011.

[16] R. Herberholz, T. Walter and H.-W. Schock, "Density of states in $CuIn(SSe)_2$ thin films from modulated photocurrent measurements", *J. Appl. Phys.*, vol. 76, pp. 2904–2911, 1994.

[17] T.P. Weiss, A. Redinger, J. Luckas, M. Mousel and S. Siebentritt, "Admittance spectroscopy in kesterite solar cells: Defect signal or circuit response", *Appl. Phys. Lett.*, vol. 102, pp. 202105-1–202105-4, 2013.

[18] T. Eisenbarth, T. Unold, R.Caballero, C.A. Kaufmann and H.-W. Schock, "Interpretation of admittance, capacitance-voltage, and current-voltage signatures in Cu(In,Ga)Se_2 thin film solar cells", *J. Appl. Phys.*, vol. 107, pp. 034509-1–034509-12, 2010.

[19] U. Reislöhner, H. Metzner, and C. Ronning, "Hopping Conduction Observed in Thermal Admittance Spectroscopy", *Phys. Rev. Lett.*, vol. 104, pp. 226403-1–226403-4, 2010.

[20] J.H. Scofield, "Effects of series resistance and inductance on solar cell admittance measurements", *Solar Energy Mater. Sol. Cell.*, vol. 37, pp. 217–233, 1995.

[21] S. Siebentritt, N. Rega, A. Zajogin and M.Ch. Lux-Steiner, "Do we really need another PL study of $CuInSe_2$", *Phys. stat. sol. (c)*, vol. 1, pp. 2304–2310, 2004.

[22] S. Siebentritt and U. Rau, *Wide-Gap Chalcopyrites*. Berlin/Heidelberg, Germany: Springer-Verlag, 2006.

[23] A. Yelon, B. Movaghar and H.M. Branz, "Origin and consequences of the compensation Meyer-Neldel law", *Phys. Rev. B*, vol. 46, pp. 12244–12250, 1992.

[24] A. Krysztopa, M. Igalson, L. Gütay, J.K. Larsen and Y. Aida, "Defect level signatures in $CuInSe_2$ by photocurrent and capacitance spectroscopy", *Thin Solid Films*, vol. 535, pp. 366–370, 2013.

[25] A.F. Tasch and C.T. Sah, "Recombination-generation and optical properties of gold acceptor in silicon", *Phys. Rev. B*, vol. 1, pp. 800–809, 1970.